A Sliding-Correlator-based SAGE algorithm for Mm-wave Wideband Channel Parameter Estimation

Xuefeng Yin[1], Yongyu He[1], Zinuo Song[1], Myung-Don Kim[2] and Hyun Kyu Chung[2]
[1]School of Electronics and Information Engineering, Tongji University, Shanghai, China
[2]Electronics and Telecommunications Research Institute, Daejeon, Republic of Korea
Email: {yinxuefeng, 1131704, 06szn}@tongji.edu.cn, {mdkim, hkchung}@etri.re.kr

***Abstract*—In this contribution, a high-resolution parameter estimation algorithm is derived based on the Space-Alternating Generalized Expectation-maximization (SAGE) principle for extracting multipath channel parameters from the output of sliding correlator (SC) which is used in millimeter-wave wideband channel measurements. By utilizing a parametric model describing the SC's output, the multipath parameters can be estimated by exploiting both low- and high-frequency components in the SC's output. Notice that conventional channel parameter estimation algorithms only make use of the time-dilated channel impulse response (CIR) calculated from the low-frequency component, and the high-frequency components, which are considered as distortions are discarded by low-pass filtering the SC's output. The algorithm proposed here can also be applied to estimate the Doppler frequencies of multipath from the SC's output containing only one observation of the time-dilated CIR, which is useful for the cases where channels change too fast to collect multiple observations of CIRs within channel coherence time. Simulations are conducted to verify the effectiveness of the proposed algorithm and evaluate its performance in terms of root mean square estimation errors.**

***Index Terms*—Mm-wave propagation channel, maximum-likelihood estimation, the SAGE algorithm, high-resolution parameter estimation, sliding correlator, low-pass filtering, and multipath.**

I. Introduction

Measurement-based channel models are important for verifying the performance of wireless communication systems in realistic propagation scenarios [1] [2]. Geometry-based stochastic channel models, such as the WINNER spatial channel models [3], IMT-Advanced models [4], and COST2100 multiple-input multiple-output (MIMO) models [5], have been proposed in various standards and widely used to generate single- and multi-link channel realizations at the carrier frequency up to 6 GHz with a bandwidth up to 100 MHz.

Recently researches on the Fifth generation (5G) wireless communications have been paid a lot of attention. The European 7th framwork project "Mobile and wireless communications Enablers for the Twenty-twenty Information Society (METIS) " announced a white paper which describes the typical applications and propagation environments considered in 5G [6]. According to the definition by the METIS project, the candidate frequency bands for 5G applications range from 0.45 to 85 GHz, and the bandwidth is from 0.5 up to 2 GHz [6]. At present, the shortage of measurement-based channel models for these frequencies, particularly in the millimeter (mm)-wave bands hinders both the progress of 5G standardization and the designing of 5G-based communication systems and networks. Characterization of the wideband channel in the mm-wave bands require extensive measurements in various environments. To lower the complexity of receiver designing and also reduce costs substantially, the sliding correlation technique has been widely adopted which outputs the time-dilated approximate of channel impulse responses (CIRs) [7], [8], [9], [10]. Since the output of the Sliding Correlator (SC) contains both the time-dilated CIR and the so-called distortion components which have higher frequencies, the Low-Pass-Filtering (LPF) or pre-filtering techniques are applied to remove the distortion components [11], [12].

However, the higher-frequency components in the SC's output prior to LPF still carry the information of channels. Thus, removing these components would waste the information that could be exploited to improve the accuracy of parameter estimation. In this paper, we derive a parametric-model-based estimation algorithm in order to make use of both the low- and high-frequency components generated by the SC. Furthermore, in the cases of time-variant channels, the time-dilated CIR needs to be calculated with the observations collected within the channel coherence time. Due to this constraint, collecting multiple CIRs by using the SC becomes impractical, especially when the sliding factor (to be introduced in Section II) is large. In this paper, we propose a generic model for the SC's output and derive the SAGE algorithm applicable for the time-variant scenarios where the observation of only one CIR is available. Simulation results illustrate the advantages of the proposed scheme over the conventional LPF-based method.

The rest of the paper is organized as follows. Section II describes the parametric signal model. In Section III, a SAGE algorithm is presented. In Section IV, simulation results illustrate the performance of the proposed algorithm. Finally conclusive remarks are addressed in Section V.

II. Signal model

As elaborated in [7], [8] and [11], the SC performs a specific cross-correlation operation e.g. between a pseudo-noise (PN) random sequence $u(t)$ with chip rate f_c and another sequence

This work was supported by the IT R&D program of MSIP/KCA, Korea. [2013-005-036-001, Wireless Channel and Frequency Characterization based on Field Measurements for Broadband Mobile Hot-Spot Applications], the China fundamental education basic research project [Polarization characterization of wireless propagation channel], the project [13510711000, System design and demo-construction for cooperative networks of high-efficiency 4G wireless communications in urban hot-spot environments] sponsored by the Science and Technology Commission of Shanghai Municipality, and the Key Program of National Natural Science Foundation of China (Grant No. 61331009).

$u'(t)$ with chip rate f_c'. According to [11], both sequences contain exactly the same chips, and the chip rates are related as $f_c' = \frac{\gamma-1}{\gamma} f_c$, where γ is called sliding factor. By sample-wise multiplying these two sequences in the time domain for multiple cycles which start with linearly increasing time-offsets and summing the products over individual cycles of $u'(t)$, a time-dilated approximate $r_u(\frac{\tau}{\gamma})$ of the autocorrelation function $r_u(\tau)$ of $u(t)$ in delay τ can be extracted from the SC's output. Generalized to the channel sounding cases where the transmitted sequence, i.e. $u(t)$, convolves with the CIR $h(\tau)$, the output of the SC after the LPF with bandwidth $B_{\mathrm{LPF},n} = [-n\frac{f_c}{\gamma}, n\frac{f_c}{\gamma}]$, $n = 1$, is the time-dilated approximate of the CIR, i.e.

$$\hat{h}\big(\frac{\tau}{\gamma}\big) = h\big(\frac{\tau}{\gamma}\big) * r_u\big(\frac{\tau}{\gamma}\big), \tag{1}$$

where $*$ denotes the convolution operation. It is widely believed that only $\hat{h}(\frac{\tau}{\gamma})$ obtained with the LPF bandwidth $B_{\mathrm{LPF},1}$ can be used to estimate the channel parameters. Whether the components obtained with $B_{\mathrm{LPF},n}$, $n > 1$ are applicable for estimating $h(\tau)$ has never been considered as far as we are concerned.

In this study, we are interested at extracting the delay and Doppler frequency dispersion of the time-variant channel which consists of M specular paths based on the SC's output that can be used to generate only observation of $\hat{h}(\frac{\tau}{\gamma})$. This is usually the case where the channel coherence time is too short for the SC to collect data long enough for observing multiple consecutive CIRs. However, the proposed models and the SAGE algorithm derived can be readily extended to the case where multiple IRs are available within the channel coherence time.

The baseband representation $r(f)$ of the received signal expressed in frequency domain can be written as

$$r(f) = \sum_{\ell=1}^{M} \alpha_\ell \exp\{-j2\pi f\tau_\ell\} u(f-\nu_\ell) + n(f), \tag{2}$$

where α_ℓ, τ_ℓ and ν_ℓ denote the complex attenuation, delay and Doppler frequency of the ℓth propagation path respectively, and $u(f)$ is the transmitted maximum-(m-)length PN sequence of L chips. When a rectangular pulse shape is applied, $u(f)$ can be written as [11]

$$u(f) = \frac{V_0}{L} \sum_{k\in\mathcal{Z}} \mathrm{sinc}(\frac{k}{L}) \delta(f - \frac{f_c k}{L}) e^{j\frac{k\pi}{L}} \sum_{i=1}^{L} (2a_i - 1) e^{-j\frac{2k\pi}{L} i}, \tag{3}$$

where V_0 is the chip magnitude, and $a_i \in [-1, 1]$, $i = i, \ldots, L$ are specified by the m-sequence. The noise component $n(f)$ in (2) is a standard white complex Gaussian random variable:

$$n(f) = w(f) \sum_{k\in\mathcal{Z}} \delta(f - \frac{f_c k}{L}), \;\; w(f) \sim \mathcal{CN}(0, N_0). \tag{4}$$

The expression $u'(f)$ for the lower chip-rate sequence $u'(t)$ is similar to $u(f)$ in (3) but with f_c substituted by f_c'. The SC's output $y(f) = r(f) * u'(f)$ is the result of convolution operation in the frequency domain, i.e.

$$y(f) = \sum_{\ell=1}^{M} \alpha_\ell p(f; \tau_\ell, \nu_\ell) + n'(f) \tag{5}$$

with

$$p(f;\tau_\ell,\nu_\ell) = \left(\frac{V_0}{L}\right)^2 \sum_{k,k'\in\mathcal{Z}} e^{-j2\pi\frac{f_c k}{L}\tau_\ell - j\frac{\pi}{L}(k+k')} \delta\left(f - \nu_\ell - \frac{f_c k + f_c' k'}{L}\right) \mathrm{sinc}\left(\frac{k}{L}\right) \mathrm{sinc}\left(\frac{k'}{L}\right) \sum_{i=1}^{L}\sum_{i'=1}^{L} \big[(2a_i - 1)(2a_{i'}' - 1) e^{-j\frac{\pi}{L}(ki + k'i')}\big] \tag{6}$$

and

$$\begin{aligned} n'(f) =& n(f) * u'(f) \\ =& \frac{V_0}{L} \sum_{k\in\mathcal{Z}} w(f) \delta\left(f - \frac{f_c k + f_c' k'}{L}\right) \mathrm{sinc}\left(\frac{k}{L}\right) e^{-j\frac{\pi}{L}k'} \sum_{i=1}^{L} (2a_i - 1) e^{-j\frac{\pi}{L}(k'i)}. \end{aligned} \tag{7}$$

The parameters $\boldsymbol{\Theta} = [\alpha_\ell, \nu_\ell, \tau_\ell; \ell = 1, \ldots, M]$ in (5) to (7) are unknown and need to be estimated given the observation $\boldsymbol{y} = [y(f); f \in (f_1, \ldots, f_N)]$, where N represents the total number of frequency bins.

III. Parameter estimation

The maximum likelihood estimate (MLE) of $\boldsymbol{\Theta}$ can be derived based on the signal models (5) to (7). However, obtaining the MLE of $\boldsymbol{\Theta}$ requires solving a $4M$-dimensional optimization problem. The computational complexity involved prohibits any practical implementation. In the following, we present the Space-Alternating Generalized Expectation-maximization (SAGE) algorithm which can iteratively update the subsets of $\boldsymbol{\Theta}$ and output the approximate of the MLE of $\boldsymbol{\Theta}$ when the estimation process converges.

We choose the subset of the parameters to be updated in each iteration of the SAGE algorithm to be $\boldsymbol{\theta}_\ell = [\alpha_\ell, \nu_\ell, \tau_\ell]$, i.e. the parameters of individual paths. The admissible hidden data $x_\ell(f)$ for estimating $\boldsymbol{\theta}_\ell$ is naturally defined as the contribution of the ℓth propagation path and the noise components, i.e.

$$x_\ell(f) = \alpha_\ell p(f; \tau_\ell, \nu_\ell) + n'(f). \tag{8}$$

In the expectation (E-) step of the ith iteration, the expectation of the loglikelihood of $\boldsymbol{\theta}_\ell$ given $\boldsymbol{y}$ and the estimates of $\boldsymbol{\Theta}$ obtained from the $(i-1)$th iteration, denoted with $\hat{\boldsymbol{\Theta}}^{[i-1]}$, can be calculated as

$$\mathrm{E}[\Lambda(\boldsymbol{\theta}_\ell)|\boldsymbol{y}, \hat{\boldsymbol{\Theta}}^{[i-1]}] \propto -\sum_{f=f_1}^{f_N} \frac{(\hat{x}_\ell^{[i-1]}(f) - \alpha_\ell p(f;\tau_\ell,\nu_\ell))^2}{\mathrm{E}[|n'(f)|^2]},$$

where $\hat{x}_\ell^{[i-1]}(f) = \mathrm{E}[x_\ell(f)|\boldsymbol{y}, \hat{\boldsymbol{\Theta}}^{[i-1]}]$ can be calculated as

$$\hat{x}_\ell^{[i-1]}(f) = y(f) - \sum_{\substack{\ell \neq \ell' \\ \ell'=1}}^{M} \hat{\alpha}_{\ell'}^{[i-1]} p(f; \hat{\tau}_{\ell'}^{[i-1]}, \hat{\nu}_{\ell'}^{[i-1]}).$$

For notational convenience, $\hat{\boldsymbol{x}}^{[i-1]}$ is used in the sequel to represent $\hat{\boldsymbol{x}}^{[i-1]} = [\hat{x}^{[i-1]}(f); f \in [f_1, \ldots, f_N]]$.

In the maximization (M-) step of the ith iteration, the estimates $\hat{\nu}_\ell^{[i]}$ and $\hat{\tau}_\ell^{[i]}$ can be calculated as

$$(\hat{\nu}_\ell^{[i]}, \hat{\tau}_\ell^{[i]}) = \arg\max_{\nu,\tau} \{\eta(\nu, \tau)\}$$

where $\eta(\nu, \tau)$ is the objective function

$$\eta(\nu, \tau) = \frac{|\boldsymbol{p}(\nu, \tau)^{\mathrm{H}} \boldsymbol{W}^{-1} \hat{\boldsymbol{x}}^{[i-1]}|^2}{\boldsymbol{p}(\nu, \tau)^{\mathrm{H}} \boldsymbol{W}^{-1} \boldsymbol{p}(\nu, \tau)}, \tag{9}$$

with $\boldsymbol{p}(\nu, \tau) = [p(f; \tau, \nu); f = f_1, \ldots, f_N]$ being a column vector and $\boldsymbol{W}$ being a diagonal matrix with its diagonal elements equal to $\mathrm{E}[|n'(f)|^2], f = f_1, \ldots, f_N$. The amplitude estimate $\hat{\alpha}_\ell^{[i]}$ can be calculated as

$$\hat{\alpha}_\ell^{[i]} = \frac{\boldsymbol{p}(\hat{\nu}_\ell^{[i]}, \hat{\tau}_\ell^{[i]})^{\mathrm{H}} \boldsymbol{W}^{-1} \hat{\boldsymbol{x}}^{[i-1]}}{\boldsymbol{p}(\hat{\nu}_\ell^{[i]}, \hat{\tau}_\ell^{[i]})^{\mathrm{H}} \boldsymbol{W}^{-1} \boldsymbol{p}(\hat{\nu}_\ell^{[i]}, \hat{\tau}_\ell^{[i]})}. \tag{10}$$

When the convergence is achieved, e.g. the parameter estimates do not change as the iteration continues, the estimation procedure is suspended, and the parameter estimates obtained in the current iteration are considered to be the final result.

IV. Simulation study

Simulations are conducted to evaluate the performance of the proposed algorithm. Table I reports the simulation settings. Figure 1 depicts the magnitude frequency spectrum and the channel power delay profile (PDP) calculated by using of the SC's output with $B_{\mathrm{LPF},n}$, $n = 1$ and 7 respectively. The synthetic channel consists of one path without noise included. It can be observed from Figure 1 that for $B_{\mathrm{LPF},1}$, the channel PDP exhibits a dominant peak located at the correct delay. For $B_{\mathrm{LPF},7}$, i.e. high-frequency components as shown in Figure 1 (c) are considered, the PDP exhibits a single peak with severe fluctuations on the top. From these results we can see that the conventional method of delay estimation, which relies on finding the maximum of channel PDP, owns larger estimation errors when the LPF bandwidth increases.

Figure 2 depicts the loglikelihood functions of delay obtained with $B_{\mathrm{LPF},n}$ as a parameter in single-path scenarios. In the simulations, the path's Doppler frequency is assumed to be known in advance. It can be observed from Figure 2 that the main-lobes of loglikelihood functions exhibit the same zero-to-zero distance regardless of $B_{\mathrm{LPF},n}$, indicating the resolution is maintained the same. However, the loglikelihood at the correct delay increases along with n. This observation indicates that enlarging the LPF bandwidth can enhance the loglikelihood for the unknown parameters.

Table I
Parameter setting of the simulations

Parameters for SC configuration	Values
Chip rate of transmitted PN sequence $u(t)$	500.00 MHz
Chip rate of PN sequence $u'(t)$ in the SC	494.62 MHz
Sliding factor γ	93
Normalized sliding factor γ/L	3.00
Number L of chips in a PN sequence	31
Over-sampling rate	2
Bandwidth $B_{\mathrm{LPF},n}$ of low-pass-filtering	$[-n\frac{f_c}{\gamma}, n\frac{f_c}{\gamma}], n = 1, \ldots, 7$
Repetition times of $u(t)$ in Tx	93
Repetition times of $u'(t)$ in Rx (SC)	92

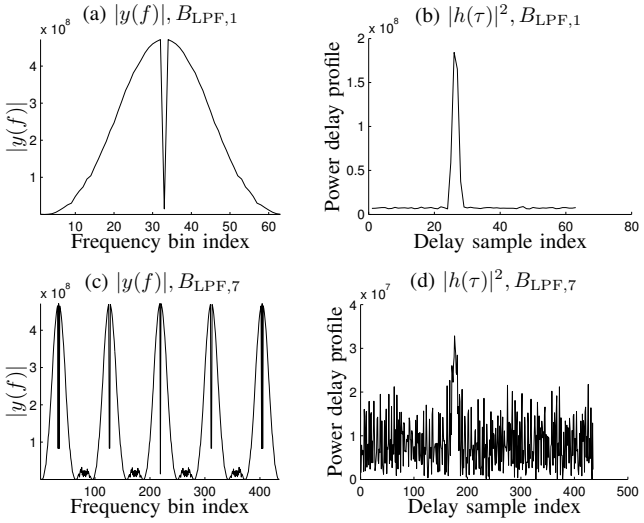

Figure 1. Magnitude frequency spectrum, power delay profile of the CIR calculated by using of the low-pass-filtered signals with the bandwidth of $B_{\mathrm{LPF},n}$, $n = 1$ and 7 respectively.

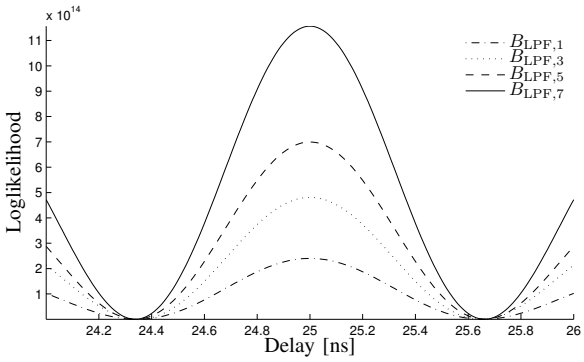

Figure 2. The loglikelihood functions of delay calculated with different settings of $B_{\mathrm{LPF},n}$ in a single-path noise-less case with the true delay equal to 25 ns. The Doppler frequency of the path is assumed to be known.

The benefits by enlarging the LPF bandwidth can also be observed in Figure 3, which depicts the root mean squared estimation error (RMSEE) of delay versus the SNR with $B_{\mathrm{LPF},n}$ as a parameter. Single-path scenarios are considered. Totally 200 Monte-Carlo simulations were conducted. The result obtained by using the conventional estimation method is also illustrated. This method searches the estimates of path delays by finding the maxima of channel PDP, which is calculated based on the SC's output with $B_{\mathrm{LPF},1}$. It can be observed from Figure 3 that for a fixed SNR, the RMSEE(τ) when the proposed algorithm is used is at least one order of magnitude lower than those obtained with the conventional method.

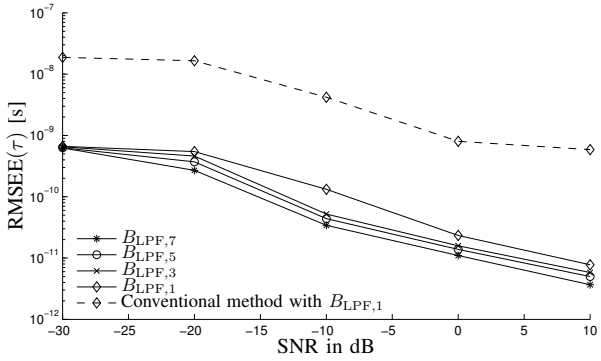

Figure 3. The RMSEE of delay versus SNR for different settings of $B_{\mathrm{LPF},n}$.

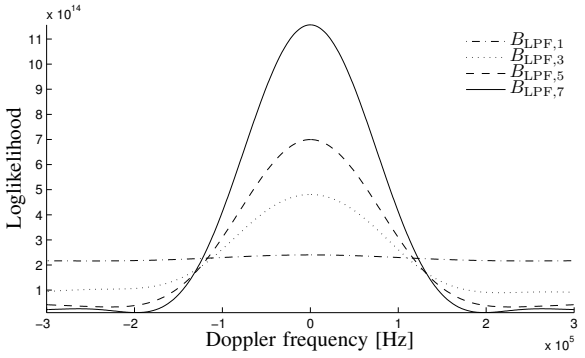

Figure 4. The loglikelihood functions of Doppler frequency calculated with different settings of $B_{\mathrm{LPF},n}$ in a single-path noise-less case with the true Doppler frequency equal to 0 Hz. The path delay is assumed to be known.

In addition, it is observed that RMSEE(τ) decreases when $B_{\mathrm{LPF},n}$ increases, indicating that the estimation accuracy can be improved by taking into account the high-frequency components when the proposed parameter estimation method is applied.

Figure 4 depicts the loglikelihood of Doppler frequency by assuming that the delay of the path is already known in single-path scenarios. The LPF bandwidth $B_{\mathrm{LPF},n}$ varies with $n = 1, 3, 5$ and 7. It can be observed from Figure 4 that the loglikelihood functions exhibit peaky main-lobes when $B_{\mathrm{LPF},n}$ increases. This indicates that by enlarging the LPF bandwidth, the accuracy of Doppler frequency estimation can be improved.

Figure 5 illustrates the RMSEE of Doppler frequency versus SNR calculated based on the Doppler frequency estimates obtained in 250 snapshots for single-path scenarios with the LPF bandwidth $B_{\mathrm{LPF},n}$, $n = 1, 3, 5$ and 7. It can be observed from Figure 5 that for fixed SNRs, the RMSEE(ν) decreases as n increases. However, the improvements in RMSEE(ν) obtained when the LPF bandwidth increases from $B_{\mathrm{LPF},1}$ to $B_{\mathrm{LPF},3}$ and from $B_{\mathrm{LPF},5}$ to $B_{\mathrm{LPF},7}$ are insignificant compared with that resulted when the bandwidth increases from $B_{\mathrm{LPF},3}$ to $B_{\mathrm{LPF},5}$. The upper floor of RMSEE(ν) observed for low SNRs in Figure 5 is due to the Doppler frequency estimation range of $[-1, 1]$ KHz specified during the simulations.

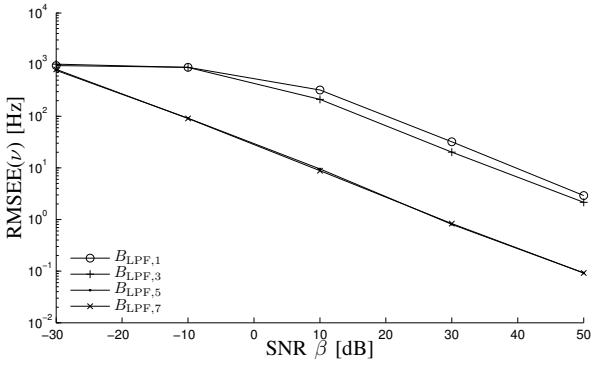

Figure 5. The RMSEEs of Doppler frequency in single-path scenarios.

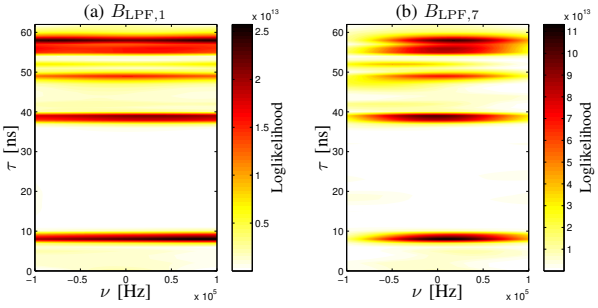

Figure 6. Loglikelihood functions $\eta(\nu, \tau)$ calculated with $B_{\mathrm{LPF},n}$, $n = 1$ and 7 in a multi-path scenario.

Figure 6 illustrates the loglikelihood functions $\eta(\nu, \tau)$ calculated with the SC's output with $B_{\mathrm{LPF},n}, n = 1$ and 7 respectively. The synthetic noise-less channel consists of a certain number of randomly generated paths with delays chosen from $[0, 62]$ ns and Doppler frequencies $[-400, 400]$ Hz. We can observe from Figure 6 that when the $B_{\mathrm{LPF},n}$ increases, the loglikelihood function becomes more peaky, and thus, the multipath components can be separated more readily. Notice that by using the SC's output that allows calculating only one CIR, the Doppler frequency estimation resolution is low. For example, by using the simulation settings in Table I, the total observation span is calculated to be $T = L\gamma/f_c = 31 \cdot 93 \cdot 2 \cdot 10^{-9} = 5.77\mu$s. Thus, the Doppler frequency estimation resolution is $1/(2T) = 43$KHz. Since the differences of Doppler frequencies of paths are empirically much less than 43KHz, it is important to jointly estimate the delay and Doppler frequency in order to resolve the paths in the delay domain. Furthermore, due to the low Doppler frequency estimation resolution, observations with high SNRs are always preferable in order to obtain less estimation errors. Our simulation results here show that the SNR should be kept beyond 10 dB and 40 dB in order to obtain RMSEE(ν) less than 10 Hz when the LPF bandwidth $B_{\mathrm{LPF},n}$ is set with $n \geq 5$ and $n \leq 3$ respectively.

The performance of the derived SAGE algorithm is evaluated in a two-path scenario, where the parameters of the paths are $(\tau_1, \nu_1, \alpha_1) = (22\text{ns}, -40\text{Hz}, 3)$, and $(\tau_2, \nu_2, \alpha_2) = (28\text{ns}, 40\text{Hz}, 1)$ respectively. The noise components are added

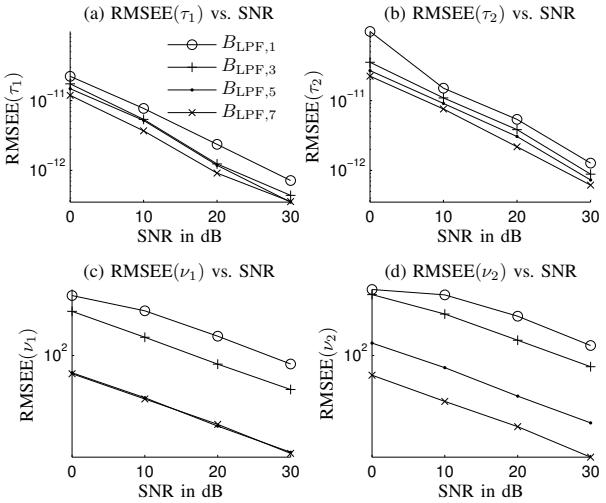

Figure 7. The RMSEEs of delay and Doppler frequency in two-path scenarios.

with $N_0 = \max(|\alpha_1|^2, |\alpha_2|^2)10^{-\zeta/10}$ where $\max(a, b)$ returns the maximum of the given arguments a and b, ζ denotes the SNR in dB. To limit the simulation times, the SAGE algorithm was executed to estimate the parameters of two paths within maximum 5 iterations. Since the true paths are set with different magnitudes, the path estimated by the SAGE algorithm with larger magnitude is considered to the estimate of the first path, and the other estimated path is the estimate of the second path, i.e. the weaker path.

Figure 7 depicts the RMSEEs of delay and Doppler frequency for the two paths versus SNR obtained from 250 simulation snapshots. It can be observed from Figure 7 that the RMSEEs of parameters for the second path are always larger than their counterparts for the first path. This is reasonable since the path 2 has lower SNR than the path 1 when synthetic channels were generated. Furthermore, by comparing Figure 7 (a) and (b) we observe that the decrease of the RMSEE of Doppler frequency for the second path when the LPF bandwidth increases from $B_{\mathrm{LPF},5}$ to $B_{\mathrm{LPF},7}$ is more significant than that obtained for the first path. We postulate that this effect of larger improvement in parameter estimation obtained for weaker paths by increasing the LPF bandwidth is due to two reasons, i.e. a higher loglikelihood of the parameters can be resulted when $B_{\mathrm{LPF},n}$ is enlarged, and additionally, the interference cancellation in the E-steps of the SAGE algorithm can be performed more efficiently, especially for paths with lower power.

V. Conclusions

In this contribution, a parametric generic model was proposed to describe the output of the sliding correlator (SC) which is usually utilized to calculate the time-dilated wideband propagation channel impulse responses (CIRs). Based on the model proposed, a SAGE algorithm was derived for extracting the delays, Doppler frequencies, and complex attenuations of multipath from the SC's output that contains only one observation of time-dilated CIR. Simulation results have shown that the conventional constraint that only the low-frequency component in the SC's output is applicable for channel estimation is unnecessary when the proposed estimation method is used. Furthermore, more high-frequency components considered, the higher the estimation accuracy can be achieved. Compared with the conventional approach which estimates the channel based on the time-dilated CIR, the proposed method is applicable not only for estimating the multipath's Doppler frequencies, but also returns more accurate estimates than the conventional method, e.g. the delay estimation errors are at least one order of magnitude less than those obtained by using the conventional method. Simulation results also demonstrated that the root mean squared estimation errors can be reduced by enlarging the bandwidth of low-pass-filtering applied in the SC. These results revealed the potential of applying the proposed high-resolution method in the SC-based parameter estimation for mm-wave wideband channel characterization.

References

[1] J. Andersen, T. Rappaport, and S. Yoshida, "Propagation measurements and models for wireless communications channels," *IEEE Communications Magazine*, vol. 33, no. 1, pp. 42–49, 1995.

[2] C. Wang, X. Cheng, and D. Laurenson, "Vehicle-to-vehicle channel modeling and measurements: recent advances and future challenges," *IEEE Communications Magazine*, vol. 47, no. 11, pp. 96–103, November 2009.

[3] *WINNER II interim channel models*, IST-4-027756 WINNER D1.1.1 Std.

[4] *Guidelines for evaluation of radio interface technologies for IMT-Advanced (12/2009)*, ITU-R M.2135-1 Std.

[5] L. Liu, C. Oestges, J. Poutanen, K. Haneda, P. Vainikainen, F. Quitin, F. Tufvesson, and P. Doncker, "The COST 2100 MIMO channel model," *IEEE Transactions on Wireless Communications*, vol. 19, no. 6, pp. 92 –99, December 2012.

[6] M. Fallgren and B. Timus, "Deliverable D1.1 Scenarios, requirements and KPIs for 5G mobile and wireless system," Project Name: Mobile and wireless communications Enablers for the Twenty-twenty Information Society (METIS) , Document Number: ICT-317669-METIS/D1.1, Tech. Rep., 2013.

[7] G. Dyer, T. Gilbert, S. Henriksen, and E. Sayadian, "Mobile propagation measurements using CW and sliding correlator techniques," in *Proceedings of IEEE Antennas and Propagation Society International Symposium*, vol. 4, 1998, pp. 1896–1899 vol.4.

[8] S. Guillouard, G. El-Zein, and J. Citerne, "High time domain resolution indoor channel sounder for the 60 ghz band," in *Proceedings of the 28th European Microwave Conference*, vol. 2, 1998, pp. 341–344.

[9] H. Xu, V. Kukshya, and T. Rappaport, "Spatial and temporal characteristics of 60-GHz indoor channels," *IEEE Journal on Selected Areas in Communications*, vol. 20, no. 3, pp. 620–630, 2002.

[10] T. Rappaport, F. Gutierrez, E. Ben-Dor, J. Murdock, Y. Qiao, and J. Tamir, "Broadband millimeter-wave propagation measurements and models using adaptive-beam antennas for outdoor urban cellular communications," *IEEE Transactions on Antennas and Propagation*, vol. 61, no. 4, pp. 1850–1859, 2013.

[11] R. Pirkl and G. Durgin, "Optimal sliding correlator channel sounder design," *IEEE Transactions on Wireless Communications*, vol. 7, no. 9, pp. 3488–3497, 2008.

[12] ——, "Revisiting the spread spectrum sliding correlator: why filtering matters," *IEEE Transactions on Wireless Communications*, vol. 8, no. 7, pp. 3454–3457, 2009.